The effect of rotational Brownian motion on Witten–Sander aggregates

H. G. E. Hentschel and J. M. Deutch
Department of Chemistry, Massachusetts Institute of Technology, Cambridge, Massachusetts 02139

Paul Meakin
Central Research and Development Department, Experimental Station, E. I. du Pont de Nemours and Company, Inc., Wilmington, Delaware 19898

(Received 10 March 1986; accepted 5 May 1986)

The effect of rotational diffusion on the growth of Witten–Sander aggregates is examined. Computer simulations of a model are analyzed where the growing aggregate rotates with a rotational diffusion constant $D_{\rm rot}(R_\parallel)\sim 1/[\tau_{\rm rot}(R_\parallel/a)^\delta]$, while the irreversibly aggregating particles jump with a diffusivity a^2/τ_0 ($\tau_0,\tau_{\rm rot}$ are the time constants for translational and rotational jumps and a is the lattice spacing). In the simulations $0.0002<(\tau_0/\tau_{\rm rot})<1600$ is varied over seven orders of magnitude. In general the aggregates are anisotropic (despite the inherent symmetry of the model) with longitudinal and transverse length scales $R_\parallel$ and $R_\perp$. On scales $r\ll R_\perp$ the cluster remains fractal, but on scales $R_\perp\ll r\ll R_\parallel$ the cluster becomes linear. Estimates of the dependence of $R_\parallel$ on N, $(\tau_0/\tau_{\rm rot})$, and δ are made and compared with the computer data. Both initial and asymptotic behavior are investigated, and several regimes of growth identified.

I. INTRODUCTION

Aggregates in nature are often not compact but have a tenuous dendritic structure[1] characterized as fractals.[2] Witten and Sander[1] introduced a model of diffusion-limited aggregation (DLA) which leads to such fractal structures. A seed particle is placed on the origin of a lattice and particles which are released isotropically from the periphery perform a random Brownian walk. If a particle reaches a nearest-neighbor site, it becomes part of the growing cluster. Computer simulations[3] have shown that the resulting aggregates are fractals, and can be characterized by a fractal dimension D which can be extracted from the relationship $N\sim R^{D(d)}$ between the number of particles N in the aggregate and its radius of gyration R. Here $\sim$ means "scales-like" and d is the embedding dimension of the Euclidean space. The same information can also be found from the correlation function

$$C(r)=\langle\rho(\mathbf{r}')\rho(\mathbf{r}'+\mathbf{r})\rangle\sim r^{D(d)-d}, \tag{1.1}$$

where $\rho(\mathbf{r})$ is the local particle density.

Though the Witten–Sander model has proved vital to our understanding, several important phenomena affecting growth have been neglected, and the model has been generalized in many directions by later studies in order to make it conform more closely to the growth processes which occur in physical systems.[3–8] For example, variable striking probability[3,4] thickens the arms of the aggregate at short scales but does not change the fractal structure at large scales. Permitting the aggregate to grow in a bath of finite concentration[5,6] causes the fractal structure to break down asymptotically after which the aggregate grows as a compact object. Similarly, if the aggregation proceeds by coagulation, where all particles may act as clusters in a medium where they collide, the model of single particle aggregation must be replaced by a model for cluster–cluster aggregation. Computer simulations have shown[7,8] that though the resulting cluster–cluster aggregates are fractal, their fractal dimension is in a completely different universality class from DLA.[9]

Rotational Brownian motion due to thermal fluctuations is another effect which may be expected to alter the structure of real aggregates in a medium. Up to the present rotational motion has not been included in the study of DLA-type growth. Therefore, in this paper we investigate the effect of rotational Brownian motion on Witten–Sander aggregates especially as regards their fractal dimension and structure. We shall see that on short scales the aggregate retains a fractal structure but there exists a dynamical symmetry breaking which creates globally anisotropic aggregates. This occurs, despite the inherently isotropic nature of the model: both the rotating aggregate and the diffusing particles have no preferred symmetry axis. This effect can be understood qualitatively. A random fluctuation in size in some direction is unstable since it tends to catch the particles diffusing in from the periphery before the rest of the aggregate. Whether this effect is transient or asymptotically relevant depends on the relationship between the rotational diffusion of the cluster and the particle diffusivity.

In Sec. II we present a scaling theory for this effect and also estimate the relative size and structure of the aggregate under different conditions of growth. The results are discussed in Sec. III.

II. THEORY

In this section we consider the effect of rotational Brownian motion on growth of a Witten–Sander aggregate by using scaling arguments on a jump model. We compare our results with computer simulations.

Assume a particle is released from the periphery and performs a Brownian walk on a lattice with spacing a, taking a jump every time interval τ_0. The aggregate is randomly rotating about its center of mass with a rotational diffusion constant $D_{\rm rot}(R_\parallel)$ where

$$D_{\rm rot}(R_\parallel)\sim[\tau_{\rm rot}(R_\parallel/a)^\delta]^{-1}. \tag{2.1}$$

Here, we assume that the aggregate is not necessarily spheri-

 0021-9606/86/162147-07$02.10

cal but has a unique symmetry $R_{\|}$ axis which is taken to be the largest principal radius of gyration; $R_{\perp}$ is the size of the other $(d-1)$ principal radii.

The computer simulations were carried out using an off lattice[3] DLA model. Both the diffusion of the mobile particle and the rotational Brownian motion of the cluster are represented by moving the particle relative to a stationary cluster. If the particle is in the vicinity of the cluster, the distance from the center of the mobile particle to the center of the closest particle on the cluster ($r_{\min}$) is obtained. The particle then follows a path consisting of a sequence of angular and translational displacements until it reaches the edge of a circle of radius $r_{\min}-1$ particle diameters from the original position of the mobile particle. The lengths of the translational and rotational displacements are a small fraction (less than 10%) of $r_{\min}-1$ and the relative probabilities of translation and rotation are calculated from the translational and rotational diffusion coefficients. When the mobile particle reaches a distance of $r_{\min}-1$ particle diameters, the new minimum distance is obtained and the process outlined above is repeated. When the mobile particle is only a small distance from a particle in the cluster (within 1/4 particle diameters in our simulations), the rotational motion is stopped and the particle takes translational steps of length 1/4 particle diameters. If one of these steps causes the mobile particle to contact one of the stationary particles in the cluster, it is moved to the position of first contact and incorporated into the growing cluster of particles. In the case of very fast rotational diffusion of the cluster, the distance from the cluster for purely translational motion and the minimum step length would have to be reduced below 1/4 particle diameters. This was not necessary in our simulations.

If the particle is outside of the region occupied by the cluster, it undergoes only translational diffusion. However, the "time" (proportional to $\Sigma_i l_i^2$ where l_i is the length of the ith step) spent outside of the region occupied by the cluster is recorded and a corresponding rotation (randomly selected from an appropriate Gaussian distribution of angles calculated from the time and the rotational diffusion coefficient) is carried out when the particle returns to the region occupied by the cluster.

Results for aggregates generated in computer simulations of the model in two dimensions for several values of $(\tau_0/\tau_{\rm rot})$ and δ are presented in Figs. 1–6. Log–log plots of the correlation function $C(r)$ at small scales are also included. Note the anisotropic nature of the clusters. The parameters τ_0, $\tau_{\rm rot}$, and the exponent δ are quantities which are fixed by choice in the computer simulation. On the basis of hydrodynamics for compact spherical objects $(d>2)$ one expects $D_{\rm rot}\sim R^{-d}$ and $D_T\sim R^{2-d}$ where D_T is the transla-

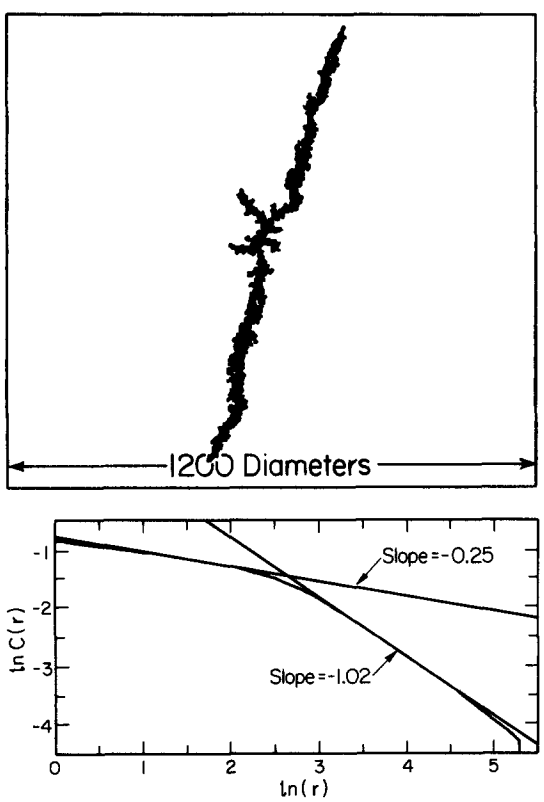

FIG. 1. (a) Cluster "b" of Table II. $\delta=0$, $(\tau_0/\tau_{\rm rot})=0.004$, $N=11\,107$. The late stage ($N_1\approx 315$, consequently $N\gg N_1$) of growth of an initially slowly rotating cluster. The remnants of the initial Witten–Sander growth (when $N\ll N_1$) can be seen at the cluster center. The cluster is growing linearly $(R_{\|}/a)\sim(\tau_0/\tau_{\rm rot})^{(D-1)/(2-\delta)}N$. (b) A log–log plot of the density correlation function $C(r)$ vs (r/a) for cluster b at small scales. The breakdown of fractal structure at $R_{\perp}$ and the crossover to linear behavior can be seen.

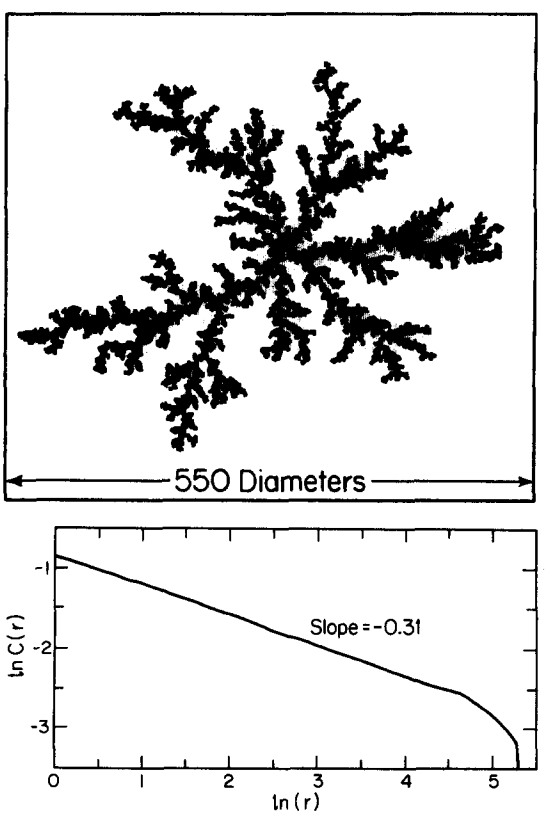

FIG. 2. (a) Cluster "f" of Table II. $\delta=1.0$, $(\tau_0/\tau_{\rm rot})=0.0025$, $N=14\,053$. The early stage ($N_1\approx 22\,153$, consequently $N<N_1$) of growth of our initially slowly rotating cluster. The cluster is almost isotropic and indistinguishable from the normal DLA. (b) A log–log plot of the density correlation function $C(r)$ vs (r/a) for cluster f. The correlation function is similar to that expected for DLA.

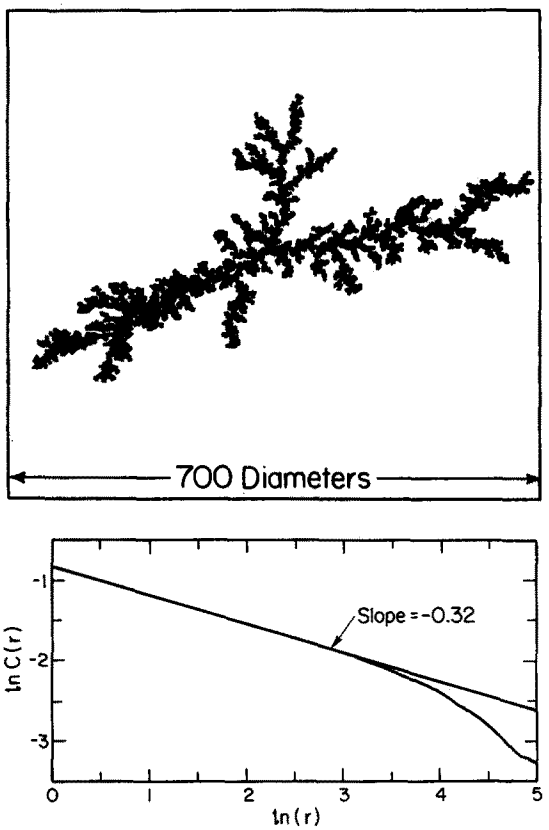

FIG. 3. (a) Cluster "g" of Table II. $\delta = 1.0$, $(\tau_0/\tau_{\rm rot}) = 0.01$, $N = 12\,461$. To be compared with Fig. 2(a). The exponent δ is the same but the cluster is at a later growth stage ($N_1 \approx 2188$, consequently $N > N_1$). The DLA structure has broken down and due to a dynamic equilibrium between particle capture at the sides and cap of the aggregate $-(R_\parallel/a) \sim [(\tau_0/\tau_{\rm rot})^{D-1}N]^{1/[\delta(D-1)+(2-D)]}$. (b) A log–log plot of the density correlation function $C(r)$ vs (r/a) for cluster g at small scales.

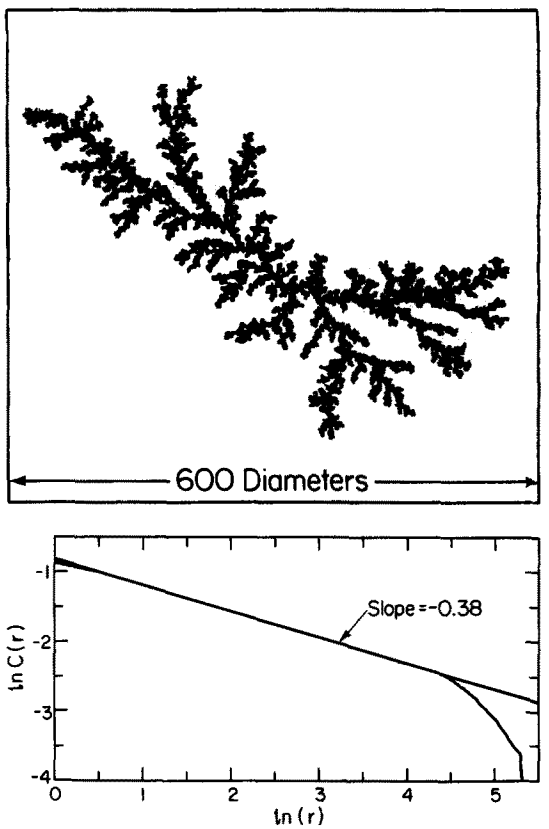

FIG. 4. (a) Cluster "k" of Table II. $\delta = 2.0$, $(\tau_0/\tau_{\rm rot}) = 1.0$, $N = 12\,811$. The marginal case $\delta = 2.0$. Perhaps the physically most realistic representation of the effect of thermal fluctuation in two dimensions as $(\tau_0/\tau_{\rm rot}) \approx 1.0$. (b) A log–log plot of the density correlation function $C(r)$ vs (r/a) for cluster K at small scales.

tional diffusion coefficient. Of course, DLA clusters are not compact. However, Chen *et al.*[10] have found for DLA clusters (without rotation) that $D_T \sim R^{-1}$ in $d = 3$ is obeyed to a surprising degree. Therefore, the identification $\delta = d$ may well be a good approximation.

It is apparent that the clusters in Figs. 1–6 can be described by two length scales $R_\parallel$ the maximum end-to-end distance and a transverse length scale $R_\perp$ which is the "thickness" of the aggregate. On length scales $r \ll R_\perp$ the aggregate appears to be Witten–Sander-like, while on scales $R_\perp \ll r \ll R_\parallel$ the cluster is one-dimensional. We note that the cluster can be covered with $(R_\parallel/R_\perp)$ blobs of size $R_\perp$. Therefore, the number of particles N in the cluster scale as

$$N \sim (R_\perp/a)^D((R_\parallel/R_\perp) \sim (R_\perp/a)^{D-1}(R_\parallel/a). \quad (2.2)$$

We can confirm that the aggregate is Witten–Sander-like on scales $r \ll R_\perp$. It is clear from the log–log plots of the correlation function that fractal behavior with DLA exponents is observed on scales $r \ll R_{\rm corr}$ where we estimate $R_{\rm corr}$ from the intercept of the two asymptotic slopes of the log-log plots of the correlation function $C(r)$. Similarly, we can estimate $(R_\perp/a)$ from the relation (2.2) and our knowledge of $(R_\parallel/a)$ and N as $(R_\perp/a) \sim [N/(R_\parallel/a)]^{1/(D-1)}$. The results are tabulated in Table I for 18 different aggregates generated in computer simulations and in Fig. 7 can be seen a log–log plot for the estimates of $R_\perp$ against $R_{\rm corr}$; in fact $R_\parallel \approx 1.4R_{\rm corr}$ is a good fit to the data. Thus Eq. (2.2) is valid and, if we could estimate one length scale for instance $R_\parallel$, we would have a full description of the aggregate.

To find how the cluster grows, we have to estimate where a particle diffusing in from the periphery is likely to strike an aggregate of longitudinal length scale $R_\parallel$, and transverse length scale $R_\perp$, performing rotational Brownian motion with a diffusion constant given by Eq. (2.1). There exist two competitive processes. These can be best understood by treating the aggregate as a cylinder. First the rotational motion will enhance the possibility of capture by the caps of the cylindrical cluster. Second, because the surface area of the sides is larger than the cap ends, this will favor capture by the cylinder sides.

These ideas can be made quantitative and a differential equation for $d \ln R_\parallel/d \ln N$ derived. First we define $P_{\rm end}$ to be the probability of the diffusing particle sticking to the cap while $P_{\rm side}$ is the probability of sticking to the sides of the cylinder

$$P_{\rm end} + P_{\rm side} = 1. \quad (2.3)$$

We now estimate $P_{\rm end}$. Rotation will increase $P_{\rm end}$ compared to the static case. We argue that $P_{\rm end}$ can be written

$$P_{\rm end} = P_{\rm static} + P_{\rm kinetic}, \quad (2.4)$$

due to two processes. Either the diffusing particle hits a clus-

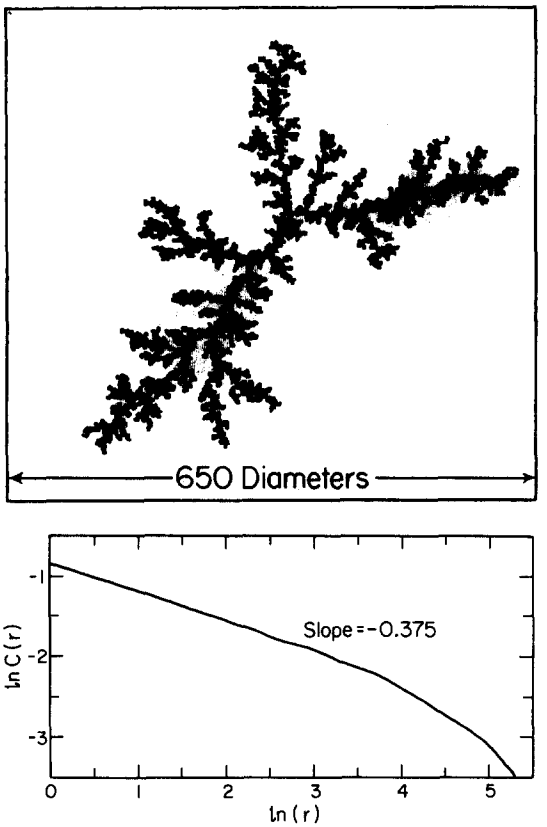

FIG. 5. (a) Cluster "q" of Table II. $\delta = 3.0$, $(\tau_0/\tau_{\rm rot}) = 100$, $N = 13\,962$. The late stage of growth of an initially quickly rotating cluster which has slowed down to such an extent that the final DLA structure has appeared ($N_1 \approx 2188$, $N_2 = 10$, consequently $N \gg N_1 \gg N_2$). No remnant of the initial linear structure can be seen as N_2 is so small. (b) A log–log plot of the density correlation formation $C(r)$ vs (r/a) for cluster q.

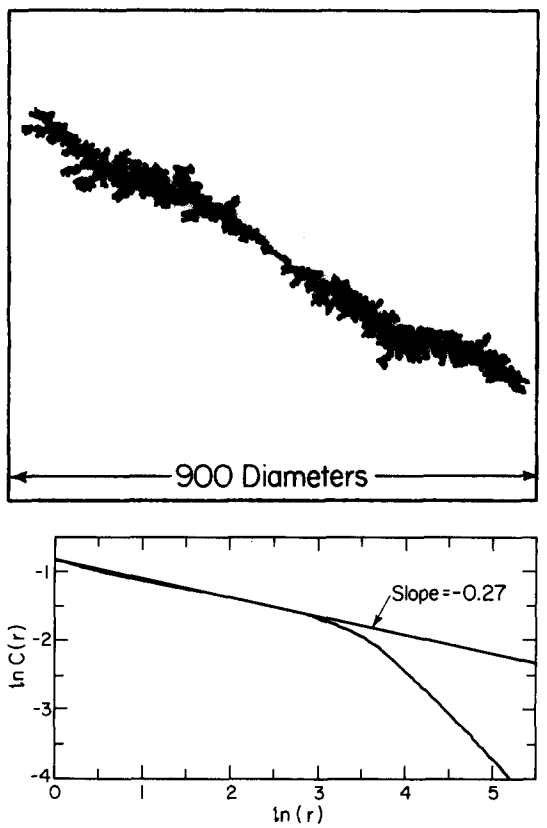

FIG. 6. (a) Cluster "r" of Table II. $\delta = 3.0$, $(\tau_0/\tau_{\rm rot}) = 1600$, $N = 12\,662$. Compare with cluster q which has the same value of δ. This is at a much earlier stage of growth. The initial rotation has only slowed down to the extent that we are in the crossover regime ($N_1 \approx 224{,}326$, $N_2 \approx 40$ consequently $N_1 \gg N \gg N_2$) between an initially linear structure and final Witten–Sander cluster. Here the remnant of the initial linear structure can be seen at the cluster center. (b) A log–log plot of the density correlation function $C(r)$ vs (r/a) for cluster r.

ter monomer by chance as it reaches a distance $R_\parallel$ from the center of mass with a probability $P_{\rm static}$ where

$$P_{\rm static} \sim (R_\perp/a)^{D-1}/(R_\parallel/a)^{d-1}, \tag{2.5}$$

which is the probability that a site in the surface of a d-dimensional sphere of radius $R_\parallel$ is occupied by one of the $(R_\perp/a)^{D-1}$ cap monomers.

Alternatively the diffusing particle reaches an empty site on the surface, but in the time τ_0 that it sits there, it gets hit by one of the randomly moving cap monomers. This occurs with a probability $P_{\rm kinetic}$, where

$$P_{\rm kinetic} \sim (\tau_0/\tau_{\rm rot})(R_\parallel/a)^{3-\delta-d}(R_\perp/a)^{D-1}$$
$$\sim (\tau_0/\tau_{\rm rot})(R_\parallel/a)^{2-\delta}P_{\rm static}. \tag{2.6}$$

Note that $(\tau_0/\tau_{\rm rot})(R_\parallel/a)^{2-\delta}$ is the ratio of the diffusivity of an aggregate monomer in the cap $\sim R_\parallel^2 D_{\rm rot}(R_\parallel)$ to the particle diffusivity $\sim a^2/\tau_0$.

To estimate $P_{\rm side}$ we argue that, as the density is the same $\sim (R_\perp/a)^{D-d}$ everywhere, the ratio of $P_{\rm side}$ to $P_{\rm static}$ is simply proportional to the surface areas of the sides of the cylinder $R_\perp^{d-2}R_\parallel$ to the surface area of the caps $R_\perp^{d-1}$ or

$$P_{\rm side} \sim (R_\parallel/R_\perp)P_{\rm static}. \tag{2.7}$$

We can now find an equation for $R_\parallel$. Roughly one out of every $\delta N \sim P_{\rm end}^{-1}$ particles stick to the end of the cylinder. This particle will increase $R_\parallel$ by $\delta R_\parallel \approx a/(R_\perp/a)^{D-1}$, or $dR_\parallel/dN \approx aP_{\rm end}/(R_\perp/a)^{d-1}$. Using Eq. (2.2) we find $d\ln(R_\parallel/a)/d\ln N \approx P_{\rm end}$. However, from Eqs. (2.3)–(2.7) we can estimate $P_{\rm end}$ and consequently

TABLE I. Conditions of growth and data for the 18 clusters analyzed in this paper.

Cluster	δ	$(\tau_0/\tau_{\rm rot})$	N	$(R_\parallel/a)$	$(R_\perp/a)$	$(R_{\rm corr}/a)$
a	0.0	0.001	12 230	830	57	37
b	0.0	0.004	11 107	1030	35	14
c	0.5	0.0002	13 072	360	219	110
d	0.5	0.0006	12 286	740	68	43
e	0.5	0.0025	12 701	1020	44	30
f	1.0	0.0025	14 053	510	145	99
g	1.0	0.01	12 461	700	75	55
h	1.5	0.09	12 732	610	95	122
i	1.5	0.25	12 333	890	52	33
j	1.5	1.0	12 320	1080	39	25
k	2.0	1.0	12 811	600	99	110
l	2.0	4.0	12 456	850	56	49
m	2.0	16.0	12 390	1030	42	25
n	2.5	9.0	13 545	630	100	110
o	2.5	25.0	12 558	740	70	60
p	2.5	100.0	12 434	1000	440	37
q	3.0	100.0	13 962	650	100	81
r	3.0	1600.00	12 662	960	48	37

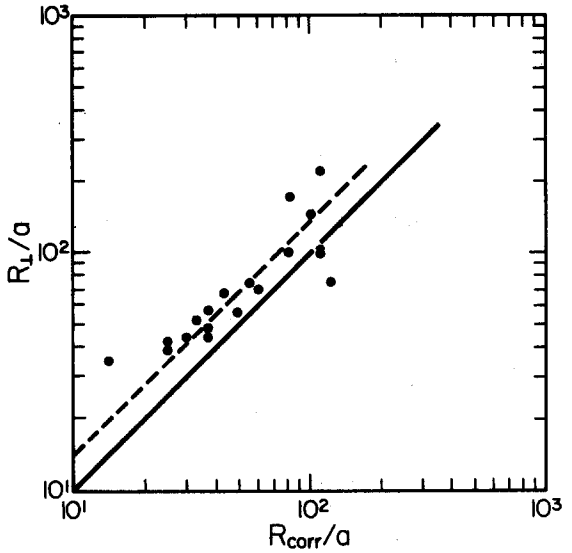

FIG. 7. A log–log plot of $(R_\perp/a)$ vs (R_{corr}/a) estimated from the data in Table I. The lines $R_\perp = R_{corr}$ and $R_\perp = 1.4\,R_{corr}$ have also been drawn.

$$\frac{d\ln(R_\parallel/a)}{d\ln N} = \frac{1 + k(\tau_0/\tau_{rot})(R_\parallel/a)^{2-\delta}}{1 + k(\tau_0/\tau_{rot})(R_\parallel/a)^{2-\delta} + (D-1)(R_\parallel/R_\perp)}, \tag{2.8}$$

where k is some constant of order unity, and the factor $(D-1)$ in front of $(R_\parallel/R_\perp)$ was found from the condition that when $(\tau_0/\tau_{rot}) = 0$ we expect DLA growth $N \sim R^D$.

Equation (2.8) can be solved subject to the initial conditions $(R_\parallel/a) = 1$ for $N = 1$ for a variety of (τ_0/τ_{rot}) and δ. However, the major features of the solutions can be seen by a qualitative analysis of Eq. (2.8).

A. $(\tau_0/\tau_{rot}) \ll 1$

For these cases the initial rotation is always very slow and initially an isotropic Witten–Sander cluster is created; as $(\tau_0/\tau_{rot})(R_\parallel/a)^{2-\delta} \ll 1$, and $(R_\parallel/R_\perp) \approx 1$ we have $d\ln(R_\parallel/a)/d\ln N = 1/D$. What happens asymptotically depends on δ.

1. $\delta > 2$

Here the rotation is always irrelevant as $(\tau_0/\tau_{rot})(R_\parallel/a)^{2-\delta} \ll 1$, $(R_\parallel/R_\perp) \approx 1$ remains valid for all N. Witten–Sander clusters are created.

2. $\delta = 2$

This is the marginal case. Actually when $\delta = 2$, Eq. (2.8) can be solved exactly with the result $(R_\parallel/a) = N^{1/D} f[N, k(\tau_0/\tau_{rot})]$ where f is the implicit solution of the equation

$$f(x,y)\,[\,y/(1+y-f(x,y)^{D/(D-1)})\,]^{(D-1)} = x^{(D-1)/D}. \tag{2.9}$$

Though Eq. (2.9) is complex, it simplifies greatly as $x \to \infty$ with the result $f^{D/(D-1)} \approx 1 + y$ or using Eq. (2.2);

$$(R_\parallel/R_\perp) \approx 1 + k(\tau_0/\tau_{rot}). \tag{2.10}$$

For $\delta < 2$ the rotation becomes relevant and the isotropic growth stage must break down. This will occur when the radius of gyration $R \approx \xi_1$, given by $(\tau_0/\tau_{rot})(\xi_1/a)^{2-\delta} \approx 1$ when $N_1 \sim (\xi_1/a)^D$ particles have been added to the growing cluster, or

$$(\xi_1/a) \approx (\tau_0/\tau_{rot})^{-1/(2-\delta)}, \qquad N_1 \approx (\tau_0/\tau_{rot})^{-D/(2-\delta)}. \tag{2.11}$$

What happens now? Both $(\tau_0/\tau_{rot})(R_\parallel/a)^{2-\delta}$ and $(R_\parallel/R_\perp)$ increase. First let us assume that as $N \to \infty$ $(\tau_0/\tau_{rot})(R_\parallel/a)^{2-\delta} \gg (R_\parallel/R_\perp)$. Thus essentially all particles are added to the caps, Eq. (2.8) gives $d\ln(R_\parallel/a)/d\ln N \approx 1$ and consequently a linear structure $(R_\parallel/a) \sim N$ is created asymptotically. Substitution of this result into our initial assumption gives $N^{2-\delta} \gg N$. Thus our assumption is only self-consistent for $\delta < 1$. Therefore we have to distinguish the regimes $1 \leqslant \delta < 2$ and $\delta < 1$.

3. $1 \leqslant \delta < 2$

For these values of δ the only alternative to $(\tau_0/\tau_{rot})(R_\parallel/a)^{2-\delta} \gg (R_\parallel/R_\perp)$ asymptotically is to assume that a dynamic equilibrium is set up between the probability of a particle being captured at the cap ends due to increasing rotation and the probability of being captured on the sides due to its increasing surface area. Thus we can expect $(\tau_0/\tau_{rot})(R_\parallel/a)^{2-\delta} \sim (R_\parallel/R_\perp)$, or

$$(R_\parallel/a) \sim [\,(\tau_0/\tau_{rot})^{D-1} N\,]^{1/[\delta(D-1)+(2-D)]}, \tag{2.12}$$

where we have used Eq. (2.2). This result is valid for $R_\parallel \gtrsim \xi_1$.

4. $\delta < 1$

For $\delta < 1$ the asymptotic behavior cannot be given by Eq. (2.12) as $1/[\delta(D-1) + (2+D)] > 1$ for $\delta < 1$. Rather, we have to assume asymptotically $(\tau_0/\tau_{rot})(R_\parallel/a)^{2-\delta} \gg (R_\parallel/R_\perp)$ and consequently as the rotation is so dominant $(R_\parallel/a) \sim (\tau_0/\tau_{rot})N$. To find the exponent α we fit this functional form to $(R_\parallel/a) \sim N^{1/D}$ at $N = N_1 \sim (\tau_0/\tau_{rot})^{-(2-\delta)/D}$ with the result

$$(R_\parallel/a) \sim (\tau_0/\tau_{rot})^{(D-1)/(2-\delta)} N. \tag{2.13}$$

Note that our two estimates of $(R_\parallel/a)$ given by Eq. (2.12) for $1 \leqslant \delta < 2$ and Eq. (2.13) for $\delta < 1$ are self-consistent as at $\delta = 1$ both give $(R_\parallel/a) \sim (\tau_0/\tau_{rot})^{(D-1)} N$.

B. $(\tau_0/\tau_{rot}) \gg 1$

For these cases the initial rotation is very fast and to begin with a linear aggregate appears with $(R_\parallel/a) \sim N$. Clearly, if the rotation slows down fast enough as $(R_\parallel/a)$ increases we would expect a breakdown in this initial linear behavior to occur as diffusing particles are absorbed on the sides of the cylinder. To estimate the length scale ξ_2 at which this breakdown occurs and the number of particles N_2 in the aggregate at this stage, we note that initially $(\tau_0/\tau_{rot})(R_\parallel/a)^{2-\delta} \gg (R_\parallel/R_\perp) \sim (R_\parallel/a)$. The linear structure breaks down when this inequality becomes and

equality or at $R_{\parallel} \sim \xi_2$ given by

$$N_2 \sim (\xi_2/a) \sim (\tau_0/\tau_{\rm rot})^{1/(\delta-1)}. \quad (2.14)$$

Clearly, the linear structure only breaks down for $\delta < 1$. The asymptotic behavior also depends on δ and therefore we consider the several possible cases separately.

1. $\delta \leqslant 1$

Here the rotation becomes even more relevant and a linear aggregate is created asymptotically.

2. $1 < \delta < 2$

For these cases the rotation is relevant in that a Witten–Sander cluster does not appear asymptotically, but not so relevant that the initial linear structure can survive. In fact, breakdown occurs for $R_{\parallel} \sim \xi_2$ and for $R_{\parallel} \gg \xi_2$ we expect the asymptotic behavior given by Eq. (2.12).

3. $\delta = 2$

The marginal case $\delta = 2$ has already been considered for all $(\tau_0/\tau_{\rm rot})$ with the asymptotic result given by Eq. (2.10): $(R_{\parallel}/a) \approx k_{\parallel} N^{1/D}$, $(R_{\perp}/a) \approx k_{\perp} N^{1/D}$, $(R_{\parallel}/R_{\perp}) \approx 1 + k(\tau_0/\tau_{\rm rot})$.

4. $\delta > 2$

Finally for $\delta > 2$ the asymptotic rotation is so weak that a Witten–Sander cluster results. Thus the growth process occurs in three states—an initial linear regime for $R_{\parallel} \ll \xi_2$ given by Eq. (2.14) where $(R_{\parallel}/a) \sim N$; then an intermediate regime $\xi_2 \ll R_{\parallel} \ll \xi_1$ where ξ_1 is given by Eq. (2.10) where the probability of sticking to the sides of the cylinder is of the same order of magnitude as at the cap ends with the result that $(R_{\parallel}/a)$ is given by Eq. (2.12); and finally a regime $R_{\parallel} \gg \xi_1$, where DLA growth $R_{\parallel} \sim R_{\perp} \sim N^{1/D} a$ is to be expected.

To test these arguments rigorously would require much more data than we have at our disposal. Instead, in Table II we give the data of 18 clusters generated on the computer together with the theoretical growth stage of each cluster and an estimate of the expected longitudinal length scale $(R_{\parallel}/a)_{\rm theor}$. Even if our arguments are correct, we could only estimate $(R_{\parallel}/a)_{\rm theor}$ within factors of the order of unity. However, the qualitative correlation in Table II of $(R_{\parallel}/a)_{\rm theor}$ and $(R_{\parallel}/a)_{\rm exp}$ is very strong. Especially since $(\tau_0/\tau_{\rm rot})$ changes by seven orders of magnitude between cluster c and cluster r. Any deviations in the correct dependence on $(\tau_0/\tau_{\rm rot})$ of $(R_{\parallel}/a)_{\rm theor}$ should be noticeable im-

TABLE II. Growth regimes for the 18 clusters.

Cluster	δ	$(\tau_0/\tau_{\rm rot})$	N	N_1	N_2	Regime	$(R_{\parallel}/a)_{\rm theor}$	$(R_{\parallel}/a)_{\rm exp}$
a	0.0	0.001	12 230	315	···	Eq. (2.13) $N \gg N_1$	1223	830
b	0.0	0.004	11 107	100	···	Eq. (2.13) $N \gg N_1$	1763	1030
c	0.5	0.0002	13 072	12 760	···	Witten–Sander $N \approx N_1$	295	360
d	0.5	0.0006	12 286	3 769	···	Eq. (2.13) $N > N_1$	454	740
e	0.5	0.0025	12 701	773	···	Eq. (2.13) $N \gg N_1$	886	1020
f	1.0	0.0025	14 053	22 153	···	Witten–Sander $N > N_1$	308	510
g	1.0	0.01	12 461	2 188	···	Eq. (2.13) $N > N_1$	570	700
h	1.5	0.09	12 732	3 059	···	Eq. (2.12) $N > N_1$	360	610
i	1.5	0.25	12 333	102	···	Eq. (2.12) $N \gg N_1$	585	890
j	1.5	1.0	12 320	1	···	Eq. (2.12) $N \gg N_1$	1169	1080
k	2.0	1.0	12 811	···	1	Eq. (2.9) $N \gg N_2$	380	600
l	2.0	4.0	12 456	···	4	Eq. (2.9) $N \gg N_2$	499	850
m	2.0	16.0	12 390	···	16	Eq. (2.9) $N \gg N_2$	865	1030
n	2.5	9.0	13 545	1 516	4	Witten–Sander $N \gg N_1 \gg N_2$	301	630
o	2.5	25.0	12 558	45 682	8.6	Eq. (2.12) $N \gg N_1 \gg N_2$	328	740
p	2.5	100.0	12 434	4.6×10^6	22	Eq. (2.12) $N \gg N_1 \gg N_2$	516	1000
q	3.0	100.0	13 962	2 188	10	Witten–Sander $N \gg N_1 \gg N_2$	307	650
r	3.0	1600.0	12 662	224 326	40	Eq. (2.12) $N \gg N_1 \gg N_2$	472	960

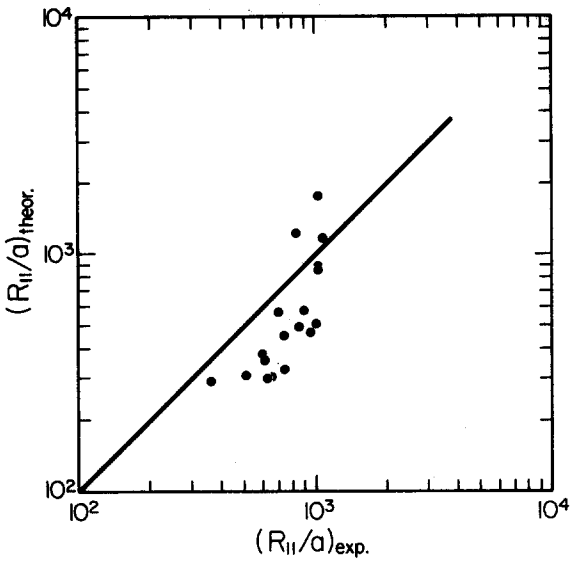

FIG. 8. A log–log plot of $(R_{\|}/a)_{\text{theor}}$ vs $(R_{\|}/a)_{\text{exp}}$ estimated from the data in Table II.

mediately. In Fig. 8 we have made a log–log plot of the data in the last two columns of Table II [the straight line in Fig. 8 represents $(R_{\|}/a)_{\text{theor}} = (R_{\|}/a)_{\text{exp}}$.] The correlation is evident.

III. DISCUSSION

In this paper we have considered the effect of rotational diffusion on diffusion-limited aggregation. Several important points have emerged from the computer simulations and our analysis.

First, the aggregates are anisotropic despite the isotropic nature of the model. Such dynamical symmetry breaking has been observed before in cluster–cluster aggregation: the model is isotropic but the resulting aggregates are "stringy" and statistically anisotropic.[11,12] But in general, situations where the global structure of the aggregate is not isotropic are due to the fact that the growth process itself has been anisotropic. Thus the structure of depositions grown on surfaces rather than from an initial seed particle have been investigated,[13–15] and these are naturally anisotropic. Similarly for a cluster grown by anisotropically diffusing particles with diffusion constants D_α in direction α on a catalyzing seed, we would expect[17] $R_\alpha \sim \sqrt{D_\alpha}$. And, even the diamond shaped fractals recently observed[18,19] are due to lattice anisotropy. Here, on the other hand, the anisotropy is due to the growth of unstable fluctuations when the rotation rate is fast enough.

Second, the asymptotic behavior depends only on δ, and as δ decreases the rotation becomes ever more relevant. For $\delta > 2$ Witten–Sander clusters are grown; while for $\delta < 1$ linear behavior is to be expected—in fact $(R_{\|}/a) \sim (\tau_0/\tau_{\text{rot}})^{(D-1)/(2-\delta)} N$. In between $1 \leqslant \delta < 2$ a dynamic equilibrium is set up between the probability of irreversible aggregation at the ends and sides of the aggregate resulting in an intermediate growth rate where $(R_{\|}/a) \sim [(\tau_0/\tau_{\text{rot}})^{(D-1)} N]^{1/(\delta(D-1)+(2-D))}$.

Third, the initial behavior depends strongly on $(\tau_0/\tau_{\text{rot}})$ and two important crossover regimes can be defined by N_1 and N_2—the number of particles in the aggregate at crossover. If $(\tau_0/\tau_{\text{rot}}) \ll 1$, then the initial growth is always isotropic, but if $\delta < 2$ then when $N_1 \sim (\tau_0/\tau_{\text{rot}})^{-D/(2-\delta)}$ particles have been added DLA behavior breaks down. For $(\tau_0/\tau_{\text{rot}}) \gg 1$ on the other hand the initial growth is always linear and this will continue unless $\delta > 1$ when after there are about $N_2 \sim (\tau_0/\tau_{\text{rot}})^{1/(\delta-1)}$ particles in the aggregate linear behavior breaks down.

Finally, the computer simulations have been carried out over seven orders of magnitude in $(\tau_0/\tau_{\text{rot}})$ and several values of δ (see Table II). These results suggest that our arguments are correct because significant deviations would be observable over this experimental range. However, for aggregates rotating due to thermal fluctuations we would expect from mode coupling $(\tau_0/\tau_{\text{rot}}) \sim 1$, and $\delta = d$. Therefore, for $d = 3$, the rotational diffusion is expected to be asymptotically irrelevant while, if $d = 2$, the situation is marginal.

ACKNOWLEDGMENT

This work is supported in part by the National Science Foundation under Grant No. CHE 8116613.

[1] T. A. Witten and L. M. Sander, Phys. Rev. Lett. **47**, 1400 (1981).
[2] B. B. Mandelbrot, *The Fractal Geometry of Nature* (Freeman, San Francisco, 1982).
[3] P. Meakin, Phys. Rev. A **27**, 1495 (1983).
[4] P. Meakin, Phys. Rev. A **26**, 647 (1982).
[5] P. Meakin and T. A. Witten, Phys. Rev. B **28**, 5632 (1984).
[6] H. G. E. Hentschel, J. M. Deutch, and P. Meakin, J. Chem. Phys. **81**, 2496 (1984).
[7] P. Meakin, Phys. Rev. Lett. **51**, 1119 (1983).
[8] M. Kolb, R. Botet, and R. Jullien, Phys. Rev. Lett. **51**, 1123 (1983).
[9] H. G. E. Hentschel and J. M. Deutch, Phys. Rev. A **29**, 1609 (1984).
[10] Z. Chen, J. M. Deutch, and P. Meakin, J. Chem. Phys. **80**, 2982 (1984).
[11] P. N. Sutherland and I. Goodarz-Nia, Chem. Eng. Sci. **26**, 2071 (1971).
[12] H. G. E. Hentschel, *Kinetics of Aggregation and Gelation* (North-Holland, Amsterdam, 1984).
[13] P. Meakin, Phys. Rev. A **27**, 2616 (1983).
[14] M. Takayama and W. Kawasaski, Phys. Lett. A **100**, 337 (1984).
[15] Z. Racz and T. Vicsek, Phys. Rev. Lett. **51**, 2382 (1983).
[16] R. Jullien, M. Kolb, and R. Botet, J. Phys. (Paris) **45**, 395 (1984).
[17] T. A. Witten, Jr., J. Phys. A **17**, L151 (1984).
[18] P. Meakin, J. Phys. A **18**, L661 (1985).
[19] R. C. Ball and R. M. Brady, J. Phys. A **18**, L809 (1985).